

Proceeding Paper

# Cycle Slip Detection of Single-Frequency Measurements in Drone Platforms <sup>†</sup>

Chan-hee Lee <sup>1</sup>  and Euiho Kim <sup>2,\*</sup> 

<sup>1</sup> Department of Mechanical Engineering, Hongik University, 94, Wausan-ro, Mapo-gu, Seoul 04066, Republic of Korea; cjessh0824@gmail.com

<sup>2</sup> Department of Mechanical & System Design Engineering, Hongik University, 94, Wausan-ro, Mapo-gu, Seoul 04066, Republic of Korea

\* Correspondence: euihokim@hongik.ac.kr

<sup>†</sup> Presented at the European Navigation Conference 2023, Noordwijk, The Netherlands, 31 May–2 June 2023.

**Abstract:** For the precise operation of Unmanned Aerial Vehicles (UAV), Real-Time Kinematic (RTK) techniques of Global Navigation Satellite System (GNSS) have been used as a positioning source. In a typical drone platform with a low-cost multi-frequency receiver, there are several dual-frequency measurements and a small set of single-frequency measurements at one time. In this paper, considering the measurement characteristics, we introduce a novel method that aims to detect a cycle slip of a small set of single-frequency measurements using dual-frequency measurements of other satellites. The performance of the proposed single-frequency cycle slip detection methods is compared with a conventional Doppler-based approach using flight test data of a drone platform.

**Keywords:** cycle slip detection; GNSS; drone flight test

## 1. Introduction

The use of a carrier phase is mandatory for precise positioning using GNSS, such as real-time kinematic (RTK) positioning or precise point positioning (PPP) [1–4]. To implement a carrier phase-based positioning, an integer ambiguity must be resolved, and its continuity should be reliably monitored. If a discontinuity of the carrier phase called a cycle slip occurs, a new integer ambiguity of the carrier phase should be found [5,6], or a cycle slip should be repaired [7,8].

In the case of single-frequency measurements, it is difficult to eliminate nuisance terms in measurements like dual-frequency measurements. Here, a typical approach is to compare a range increment from a Doppler frequency and one from carrier phase measurements, referred to as Doppler-aided cycle slip detection (DACSD) [9,10]. While Doppler measurements are immune to cycle slips, they have a high noise level that makes it difficult to detect small cycle slips. Instead of using Doppler measurements, some other approaches used an inertial measurement unit, which would make a cycle slip detection problem more complicated [11,12].

Nowadays, dual-frequency GNSS receivers are typically installed in a small UAV platform. However, a lower-grade GNSS antenna and receiver on a small UAV platform and a dynamic motion with vibrations during flights often lead to unexpected cycle slips and poor detection performance. Also, a fair amount of single-frequency measurements, along with some dual-frequency measurements, are typically observed from a dual-frequency receiver on a small UAV platform.

In the case of mixed single- and dual-frequency measurements, rather than applying a Doppler-aided cycle slip detection method like the prior works, this study proposes a novel single-frequency cycle slip detection method based on UAV velocity and receiver clock drift estimates from dual-frequency carrier measurements, providing a lower noise level in cycle slip detection test statistics.



**Citation:** Lee, C.-h.; Kim, E. Cycle Slip Detection of Single-Frequency Measurements in Drone Platforms. *Eng. Proc.* **2023**, *54*, 13. <https://doi.org/10.3390/ENC2023-15436>

Academic Editor: Tom Willems and Okko Bleeker

Published: 29 October 2023



**Copyright:** © 2023 by the authors. Licensee MDPI, Basel, Switzerland. This article is an open access article distributed under the terms and conditions of the Creative Commons Attribution (CC BY) license (<https://creativecommons.org/licenses/by/4.0/>).

The structure of the paper is as follows. Section 2 presents the prior DACSD and introduces a novel cycle slip detection algorithm for the mixed single- and dual-frequency measurements. Section 3 presents flight test results, followed by the conclusions.

## 2. Cycle Slip Detection Methods and Proposed Approach for Single-Frequency Measurements

In this section, we briefly review DACSD as a prior representative method and suggest a cycle slip detection algorithm for single-frequency measurement that utilizes only the carrier phase measurement.

### 2.1. Doppler-Aided Cycle Slip Detection Method for Single-Frequency Measurements

GNSS measurement models of a receiver are

$$\begin{aligned} \lambda_i \phi_i &= r - I_i + T + (c\delta t_u - c\delta t^s) + \lambda_i N_i + \varepsilon_\phi, \\ d_i &= \frac{d}{dt}(\phi_i) = -\frac{1}{\lambda_i} [\dot{r} + (c\delta \dot{t}_u - c\delta \dot{t}^s) + \varepsilon_d] \end{aligned} \quad (1)$$

where  $\phi$  represents a carrier measurement,  $r$  is the actual distance between a satellite and a user,  $I$  is an ionospheric delay error, and  $T$  is a tropospheric delay error. GNSS receiver and satellite clock errors are  $\delta t_u$  and  $\delta t^s$ , respectively.  $c$  is the speed of light.  $\lambda$  is the wavelength of a carrier, and  $N$  is an integer ambiguity in a carrier phase measurement.  $\varepsilon$  is the noise of each measurement.  $d$  is a Doppler measurement, which is equal to the time derivative of the carrier measurement. The subscript  $i$  denotes the frequency of each measurement.

Doppler measurements have been typically used to detect a cycle slip for single-frequency measurement. A Doppler is an apparent frequency change in a wave and is caused by the relative motion between a satellite and a user. An integrated Doppler frequency shift over some time period is equal to a carrier measurement change such that [13]

$$\Delta\phi_i = \phi_i(k) - \phi_i(k-1) = \int_{k-1}^k f_d dt, \quad (2)$$

where  $k$  is the current epoch, and  $f_d$  is an instantaneous Doppler frequency between a receiver and a satellite. If the time interval between epochs is short, (2) can be expressed as

$$\int_{k-1}^k f_d dt \approx \frac{d_i(k) + d_i(k-1)}{2} \cdot \Delta t + \varepsilon_{\Delta\phi_i}, \quad (3)$$

where  $d_i$  is a coarse Doppler shift measured by a receiver, which is immune to a cycle slip.  $\Delta t$  represents the time interval between successive epochs.  $\varepsilon_{\Delta\phi_i}$  includes nuisance errors like carrier phase measurements and noise. The shorter the time interval between successive epochs, the smaller the error caused by the Doppler measurement [9].

If there is no cycle slip between two epochs, the difference of carrier phase measurement should be equal to the integrated Doppler measurements. However, these two values will have a significant difference when there is a cycle slip because the integer ambiguity in the carrier phase measurement at the two epochs is no longer the same. Note that the Doppler measurements,  $d$ , are not impacted by a carrier phase cycle slip.

Therefore, a cycle slip can be inferred from the following

$$T_{MDACSD} = \Delta\phi_i^s - \left\{ \frac{d_i^s(k) + d_i^s(k-1)}{2} \cdot \Delta t \right\}, \quad (4)$$

where the superscript  $s$  refers to the satellite from which the signal is transmitted.

The DACSD method has the advantage of being able to detect cycle slips even in a single-frequency environment. Additionally, unlike the cycle slip detection method that

detects through a differential method between frequencies or receivers, we can identify a specific frequency or measurement at which a cycle slip occurs. However, the noise level of the test statistics is high, making it difficult to detect a small cycle slip.

### 2.2. Proposed Single-Frequency Cycle Slip Detection for Small UAV Platforms

In this section, we propose a time-difference carrier phase (TDCP) combination method that better detects a cycle slip of single-frequency carrier measurements with a lower noise level than Doppler measurements. The TDCP combination method uses the differential value of the carrier phase measurement and can be expressed as

$$\lambda_i \cdot \frac{\phi_i^s(k) - \phi_i^s(k-1)}{\Delta t} \approx \lambda_i \dot{\phi}_i^s = (\mathbf{v}^s - \mathbf{v}) \cdot \mathbf{1}^s + \dot{b} + \varepsilon_{\dot{\phi}_i^s}, \tag{5}$$

where  $\mathbf{v}^s$  is the satellite velocity vector,  $\mathbf{v}$  is the user velocity vector, and  $\dot{b}$  is change rate in a receiver clock. The rates of ionospheric and tropospheric delay are assumed to be negligible.  $\varepsilon_{\dot{\phi}_i^s}$  is the combined noise term during measurement interval, and  $\mathbf{1}^s$  is a line-of-sight vector of the satellite  $s$ . (5) can be rearranged as below

$$\lambda_i \cdot \frac{\phi_i^s(k) - \phi_i^s(k-1)}{\Delta t} - \mathbf{v}^s \cdot \mathbf{1}^s = -\mathbf{v} \cdot \mathbf{1}^s + \dot{b} + \varepsilon_{\dot{\phi}_i^s}, \tag{6}$$

Here, the left-hand side of (6) represents a value that we can calculate or obtain through measurements. The receiver velocity vector and receiver time drift value on the right-hand side are unknown and need to be estimated with a set of dual frequency measurements. When (6) is expressed in a matrix form with two frequencies, it can be represented as

$$\mathbf{Y}_{\text{dual}} = \mathbf{G}\mathbf{X} + \varepsilon_{\dot{\phi}^s}, \tag{7}$$

where  $\mathbf{Y}_{\text{dual}} = \begin{bmatrix} \lambda_i \cdot \frac{\phi_1^1(k) - \phi_1^1(k-1)}{\Delta t} - \mathbf{v}^1 \cdot \mathbf{1}^1 \\ \vdots \\ \lambda_i \cdot \frac{\phi_2^m(k) - \phi_2^m(k-1)}{\Delta t} - \mathbf{v}^m \cdot \mathbf{1}^m \end{bmatrix}$ ,  $\mathbf{G} = \begin{bmatrix} -\mathbf{1}^1 & 1 \\ \vdots & \vdots \\ -\mathbf{1}^m & 1 \end{bmatrix}$ , and  $\mathbf{X} = \begin{bmatrix} \mathbf{v} \\ \dot{b} \end{bmatrix}$ . Here,  $\mathbf{X}$  is estimated by pseudo-inverse using matrix  $\mathbf{Y}$  and matrix  $\mathbf{G}$

$$\hat{\mathbf{X}} = (\mathbf{G}^T \mathbf{G})^{-1} \mathbf{G}^T \mathbf{Y}_{\text{dual}}. \tag{8}$$

In this method, the measurements used for the user velocity and receiver clock error rate estimation should be free of any cycle slips. Therefore, we only used  $m$  dual-frequency measurements that have passed the dual-frequency carrier phase (DFCP) combination, which is often referred as a geometry-free method [14]. This is because the data that have passed through DFCP are highly likely to be free of cycle slips. Then, the  $\hat{\mathbf{X}}$  is applied for the cycle slip detection of  $s$  single-frequency carrier phase measurement as follows:

$$T_{TDCP} = \lambda_i \cdot \frac{\phi_i^s(k) - \phi_i^s(k-1)}{\Delta t} - \mathbf{v}^s \cdot \mathbf{1}^s - [-\mathbf{1}^s \quad 1] \cdot \hat{\mathbf{X}}. \tag{9}$$

When there are no cycle slips,  $T_{TDCP}$  includes noise in carrier phase as well as estimated errors in  $\hat{\mathbf{X}}$ . An experimental distribution of  $T_{TDCP}$  is addressed in later sections.

The TDCP combination method has the advantage of being able to detect a small cycle slip even in single-frequency measurements. In contrast to the DFCP method, it is possible to specify the measurement in which cycle slip has occurred. Compared to DACSD, the noise level of the proposed TDCP is reduced by using the differential value of the carrier

measurement. For this reason, the TDCP approach detects a smaller cycle slip and its false alarm is relatively lower than the one of DACSD.

### 3. Results

We collected data via flight tests and set a threshold for each cycle slip method with the flight test data. The flight tests were conducted at Hongik University’s 4th Industrial Revolution Campus located in Hwaseong, South Korea. During flight, dual-frequency measurements of GPS, Galileo, and Beidou constellations were collected at 1Hz rate. Each flight took approximately 10 min to complete, and a total of 45 flight tests were conducted. Our testbed of a small UAS was based on a S550 frame shown in Figure 1a. The receiver and antenna onboard the testbed were Ublox ZED-F9P and Trimble AV17, respectively. The speed of the UAV ranged from 1 to 6 m/s.

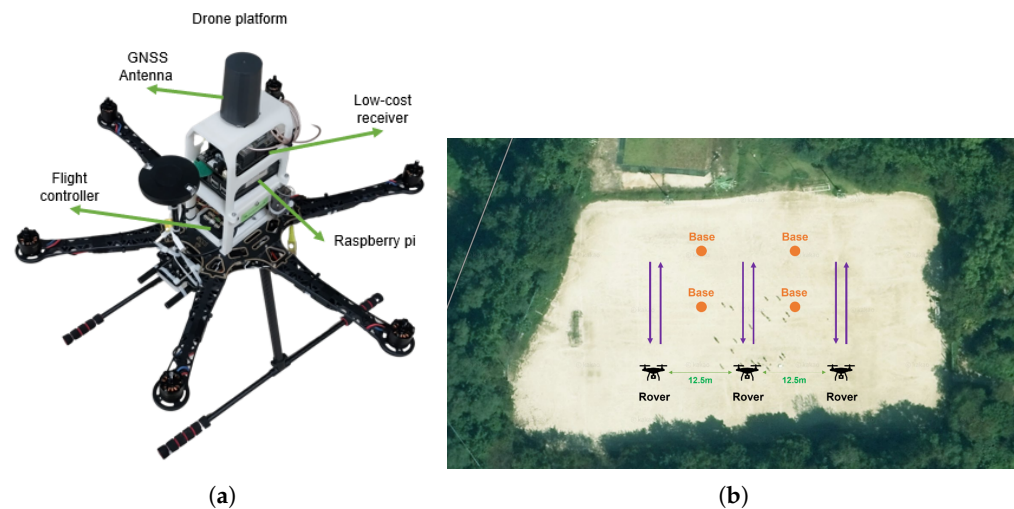


**Figure 1.** Hexacopter drone platform and flight test set-up. (a) Hexacopter drone platform with GNSS Antenna, flight controller, Ublox F9P receiver, and raspberry-pi board. (b) Trajectory of three drones during flight test.

Figure 2 shows the test statistics of DACSD and TDCP based on the flight test data. To establish a criterion for determining the occurrence of actual cycle slips, we adopted the results of the DFCP method by using dual-frequency carrier phase measurements only. Table 1 lists the number of false alarms and missed detection of cycle slips resulted from the DACSD and TDCP methods. There were no false alarms in the TDCP combination. On the other hand, in the case of DACSD, it can be observed that false alarms have occurred in many cases. Table 2 shows the number of false alarms and missed detection of simulated cycle slips injected to flight test data. For the smaller cycle slip of one wavelength, TDCP performs significantly better than DACSD.

**Table 1.** Performance comparison of MDACSD and DFCP in the aspects of false alarm and missed detection of flight data.

| Method | False Alarm Rate | Missed Detection Rate | Data    |
|--------|------------------|-----------------------|---------|
| DFCP   | 0%               | 0%                    | 738,612 |
| DACSD  | 22.4913%         | 0.058669%             | 738,612 |
| TDCP   | 0%               | 0.025206%             | 738,612 |

**Table 2.** Performance comparison of DACSD and DFCP in the aspects of missed detection through injected cycle slips.

| Dataset | Injected Cycle Slip of 1 Wavelength |       | Injected Cycle Slip of 2 Wavelength |       | No. of Simulation |
|---------|-------------------------------------|-------|-------------------------------------|-------|-------------------|
|         | TDCP                                | DACSD | TDCP                                | DACSD |                   |
| 1       | 952                                 | 0     | 952                                 | 291   | 959               |
| 2       | 711                                 | 0     | 711                                 | 302   | 711               |
| 3       | 1190                                | 0     | 1190                                | 288   | 1190              |
| 4       | 1080                                | 0     | 1080                                | 318   | 1080              |

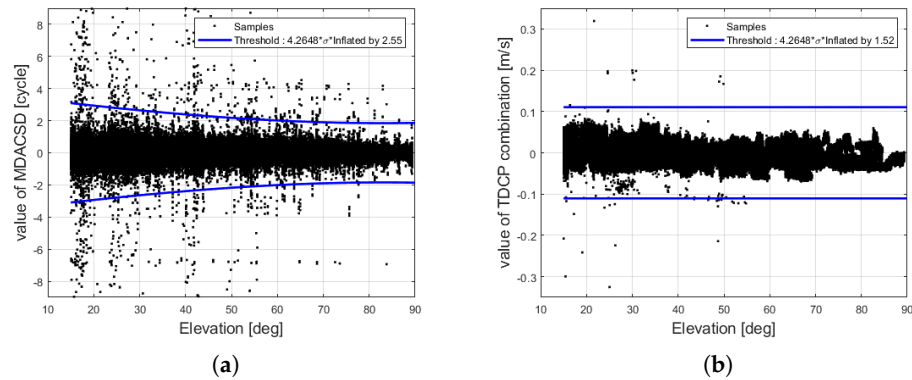


**Figure 2.** Test statistics from the flight test data. The outliers much beyond the threshold were removed in the process of determining the thresholds. (a) The DACSD combination. (b) The TDCP combination.

#### 4. Conclusions

We introduced a novel cycle slip detection method for single-frequency measurements using mixed dual- and single-frequency measurements. This method could result in more precise cycle slip test statistics compared to previous Doppler-based approaches. Our test results based on flight test data confirmed that the proposed TDCP approach provides lower false alarms and missed detection rates than Doppler-based approaches. Therefore, using this approach is advantageous in the RTK process as it allows a tighter cycle slip check on the set of single-frequency measurements obtained along with dual-frequency measurements.

**Author Contributions:** C.-h.L. developed algorithm and analyzed flight test data. E.K. provided advices throughout this research. All authors have read and agreed to the published version of the manuscript.

**Funding:** This research was supported by the Unmanned Vehicles Core Technology Research and Development Program through the National Research Foundation of Korea (NRF) and the Unmanned Vehicle Advanced Research Center (UVARC) funded by the Ministry of Science and ICT, Republic of Korea (No. 2020M3C1C1A01086407). This work was also supported by Future Space Navigation & Satellite Research Center through the National Research Foundation funded by the Ministry of Science and ICT, Republic of Korea (2022M1A3C2074404).

**Institutional Review Board Statement:** Not applicable.

**Informed Consent Statement:** Not applicable.

**Data Availability Statement:** Data sharing is not applicable to this article.

**Conflicts of Interest:** The authors declare no conflict of interest. The funders had no role in the design of the study; in the collection, analyses, or interpretation of data; in the writing of the manuscript; or in the decision to publish the results.

## References

1. Vollath, U.; Landau, H.; Chen, X.; Doucet, K.; Pagels, C. Network RTK versus single base RTK—understanding the error characteristics. In Proceedings of the 15th International Technical Meeting of the Satellite Division of the Institute of Navigation (ION GPS 2002), Portland, OR, USA, 24–27 September 2002.
2. Rizos, C. Alternatives to current GPS-RTK services and some implications for CORS infrastructure and operations. *GPS Solut.* **2007**, *11*, 151–158. [[CrossRef](#)]
3. Bisnath, S.; Gao, Y. Current state of precise point positioning and future prospects and limitations. *Obs. Our Chang. Earth* **2009**, *133*, 615–623.
4. Zumberge, J.F.; Heflin, M.B.; Jefferson, D.C.; Watkins, M.M.; Webb, F.H. Precise point positioning for the efficient and robust analysis of GPS data from large networks. *J. Geophys. Res. Solid Earth* **1997**, *102*, 5005–5017. [[CrossRef](#)]
5. Xu, G.; Xu, Y.; Xu, G.; Xu, Y. *GPS: Theory, Algorithms and Applications*, 3rd ed.; Springer: Berlin/Heidelberg, Germany, 2016; pp. 229–261.
6. Yoon, Y.; Lee, B.; Heo, M. Multiple Cycle Slip Detection Algorithm for a Single Frequency Receiver. *Sensors* **2022**, *22*, 2525. [[CrossRef](#)] [[PubMed](#)]
7. Cai, C.; Liu, Z.; Xia, P.; Dai, W. Cycle slip detection and repair for undifferenced GPS observations under high ionospheric activity. *GPS Solut.* **2013**, *17*, 247–260. [[CrossRef](#)]
8. Li, T.; Melachroinos, S. An enhanced cycle slip repair algorithm for real-time multi-GNSS, multi-frequency data processing. *GPS Solut.* **2019**, *23*, 1–11. [[CrossRef](#)]
9. Zhao, J.; Hernández-Pajares, M.; Li, Z.; Wang, L.; Yuan, H. High-rate Doppler-aided cycle slip detection and repair method for low-cost single-frequency receivers. *GPS Solut.* **2020**, *24*, 1–13. [[CrossRef](#)]
10. Ren, Z.; Li, L.; Zhong, J.; Zhao, M.; Shen, Y. A real-time cycle-slip detection and repair method for single frequency GPS receiver. *Int. Proc. Comput. Sci. Inf. Technol.* **2011**, *17*, 224–230.
11. Colombo, O.L.; Bhapkar, U.V.; Evans, A.G. Inertial-aided cycle-slip detection/correction for precise, long-baseline kinematic GPS. In Proceedings of the 12th International Technical Meeting of the Satellite Division of The Institute of Navigation (ION GPS 1999), Nashville, TN, USA, 14–17 September 1999; pp. 1915–1922.
12. Takasu, T.; Yasuda, A. Cycle slip detection and fixing by MEMS-IMU/GPS integration for mobile environment RTK-GPS. In Proceedings of the 21st international technical meeting of the satellite division of the Institute of Navigation (ION GNSS 2008), Savannah, GA, USA, 16–19 September 2008; pp. 64–71.
13. Hernández-Pajares, M.; Juan, J.M.; Sanz, J.; Aragón-Àngel, À.; García-Rigo, A.; Salazar, D.; Escudero, M. The ionosphere: Effects, GPS modeling and the benefits for space geodetic techniques. *J. Geod.* **2011**, *85*, 887–907. [[CrossRef](#)]
14. Dai, Z. MATLAB software for GPS cycle-slip processing. *GPS Solut.* **2012**, *16*, 267–272. [[CrossRef](#)]

**Disclaimer/Publisher’s Note:** The statements, opinions and data contained in all publications are solely those of the individual author(s) and contributor(s) and not of MDPI and/or the editor(s). MDPI and/or the editor(s) disclaim responsibility for any injury to people or property resulting from any ideas, methods, instructions or products referred to in the content.